ISSN 0021-3640, JETP Letters, 2015, Vol. 101, No. 8, pp. 513–518. © Pleiades Publishing, Inc., 2015.
Original Russian Text © D.A. Mylnikov, V.V. Belykh, N.N. Sibeldin, V.D. Kulakovskii, C. Schneider, S. Höfling, M. Kamp, A. Forchel, 2015, published in Pis'ma v Zhurnal Eksperimental'noi i Teoreticheskoi Fiziki, 2015, Vol. 101, No. 8, pp. 569–574.

Dynamics of Spatial Coherence and Momentum Distribution of Polaritons in a Semiconductor Microcavity under Conditions of Bose–Einstein Condensation

D. A. Mylnikov[a, b], V. V. Belykh[a], N. N. Sibeldin[a], V. D. Kulakovskii[c], C. Schneider[d], S. Höfling[d], M. Kamp[d], and A. Forchel[d]

[a] *Lebedev Physical Institute, Russian Academy of Sciences, Moscow, 119991 Russia*
e-mail: belykh@lebedev.ru

[b] *Moscow Institute of Physics and Technology (State University), Dolgoprudnyi, Moscow region, 141700 Russia*

[c] *Institute of Solid State Physics, Russian Academy of Sciences, Chernogolovka, Moscow region, 142432 Russia*

[d] *Technische Physik, Physikalisches Institut and Wilhelm Conrad Röntgen Research Center for Complex Material Systems, Universität Würzburg, D-97074 Würzburg, Germany*

Received March 10, 2015; in final form, March 16, 2015

The dynamics of spatial coherence and momentum distribution of polaritons in the regime of Bose–Einstein condensation in a GaAs microcavity with embedded quantum wells under nonresonant excitation with picosecond laser pulses are investigated. It is shown that the establishment of the condensate coherence is accompanied by narrowing of the polariton momentum distribution. At the same time, at sufficiently high excitation densities, there is significant qualitative discrepancy between the dynamic behavior of the width of the polariton momentum distribution determined from direct measurements and that calculated from the spatial distribution of coherence. This discrepancy is observed at the fast initial stage of the polariton system kinetics and, apparently, results from the strong spatial nonuniformity of the phase of the condensate wavefunction, which equilibrates on a much longer time scale.

DOI: 10.1134/S0021364015080111

Polaritons in semiconductor microcavities with embedded quantum wells (QWs), which are quasiparticles corresponding to mixed exciton–photon states in these heterostructures, represent a unique system for studying Bose–Einstein condensation (BEC). The effective mass of microcavity polaritons near the bottom of the lower dispersion branch is $\sim 10^{-4}$ of the free-electron mass, which makes possible polariton BEC at high temperatures, even up to room temperature [1]. After the demonstration of BEC in CdTe microcavities in 2006 [2], a number of interesting effects related to this phenomenon were investigated, including quantum vortices [3], the superfluidity of the polariton condensate [4], the Josephson effect [5], the spin Meissner effect [6], polariton solitons [7], and the optical spin Hall effect [8]. Very recently, an electrically pumped polariton laser working at room temperature was demonstrated [9].

One of the main characteristics of a Bose condensate is spatial coherence, i.e., the constancy of the phase of the condensate wavefunction over distances exceeding the thermal de Broglie wavelength. In this context, the dynamics of the establishment of coherence in the process of the condensate formation is an interesting issue, which was investigated in [10–12]. In particular, it was found in [12] that, in the process of formation of the polariton condensate, coherence expands with a constant velocity of $\sim 10^8$ cm/s.

Here, for the first time, the dynamics of the spatial distribution of coherence and the corresponding dynamics of the polariton momentum distribution are investigated simultaneously. The relationship between these distributions is discussed.

The structure under study is a GaAs microcavity with the top and bottom Bragg mirrors consisting of 32 and 36 pairs of AlAs/$Al_{0.13}Ga_{0.87}As$ layers, respectively. Embedded in the microcavity were 12 GaAs/AlAs 7-nm-wide QWs. The Rabi splitting and the Q factor of the structure were 4.5 meV and about 7000, respectively. The detuning between the photon and exciton modes was about –6 meV. In all experiments, the sample temperature was 10 K. The sample was excited by a Ti:sapphire laser emitting a periodic train of 2.5-ps-long pulses at a repetition rate of 76 MHz. The excitation laser beam was focused in a spot 20–30 μm in diameter. The excitation photon energy was 10–20 meV higher than the energy of the bottom of the exciton mode.

The degree of spatial coherence was measured using the Young double-slit experiment scheme [12, 13]. An enlarged image of the sample with a magnification of about 13 was obtained using two converging lenses ($F_1 \approx 1$ cm and $F_2 \approx 10$ cm) with coinciding focal planes. A metal-coated plate with a pair of 5-μm-wide transparent slits was placed in the plane of this image. The slit spacing varied from 20 to 160 μm. The chosen slit pair selected two regions in the image of the spot, and the pattern formed by the interference of radiation emitted from these two regions was imaged by a third lens onto the entrance slit of a spectrometer set to the zeroth diffraction order and coupled to a streak camera.

To measure the distribution of polaritons in momentum space (k space), the plate with slits was removed from the above setup. Then, owing to the presence of the third lens, radiation emitted by the microcavity at a certain angle θ to the normal of the sample surface and, thus, corresponding to polaritons with a wave vector $k = (\omega/c)\sin\theta$ was imaged onto a certain point at the slit of the spectrometer and, thus, of the streak camera. The time resolution of the system in our measurements was 10 ps.

Another quantity determined in our experiments was the total number of polaritons N occupying the states near the bottom of the lower polariton branch (LPB). This was attained by measuring the power of radiation emitted by the sample. The procedure of determining N is described in detail in [12].

As the pump power was increased above $P_0 \approx 750$ W/cm^2, a threshold-like increase in the intensity of photoluminescence (PL) emitted at small angles with respect to the normal took place, giving evidence of the onset of the macroscopic occupancy of the states near the LPB bottom. This is illustrated by Fig. 1a, which shows the PL spectra recorded at different angles at a pump density $P = 1.2P_0$. The positions of the spectral lines are shown by asterisks. The angular dependence of these positions describes a part of the dispersion curve corresponding to the LPB states in the strong-coupling regime.

Above the threshold pump density, measurements in the Young scheme reveal an interference pattern formed by radiation emitted from the regions of the spot selected by the two slits. This gives evidence of the onset of spatial coherence and the BEC of polaritons. The dynamics of the interference pattern for the cases where the emitting regions are spaced by $\Delta x = 5$ and 11 μm is shown in Fig. 1b. In these experiments, the sample image was adjusted with respect to the slits in such a way that the intensities of light collected from each of the slits were the same. Then, the degree of spatial coherence $g^{(1)}$ equaled the interference pattern visibility, which was calculated by performing a Fourier transform. The dependences of the coherence function on the distance Δx for different times after the excitation pulse are shown in Fig. 1c. The coherence length r_c was determined as the distance at which $g^{(1)}(r_c) = 1/e$. To calculate r_c, the dependence of $g^{(1)}(\Delta x)$ was approximated by exponential functions, also shown in Fig. 1c.

Figure 2 shows the kinetic dependences of the coherence length r_c and the total number N of polaritons near the bottom of the LPB. For excitation densities slightly exceeding the BEC threshold density P_0, the slow rise and decay of N with a characteristic time of 50 ps is accompanied by qualitatively similar variation in r_c. For densities considerably higher than P_0, the kinetics of N clearly features two regions: the initial stage with a total duration of about 50 ps and the subsequent stage of slower decay. At the first (initial) stage, the kinetics of r_c follows that of N: an increase in N is accompanied by an increase in r_c, and a drop in N is accompanied by a decrease in r_c. A characteristic maximum in the kinetics of r_c is attained simultaneously with the maximum in the number of polaritons. At the second stage, the dynamics of r_c changes abruptly. There appears a plateau, i.e., an interval of time during which r_c shows almost no decrease. This interval is as long as 100 ps for $P = 6.9P_0$. At longer times, r_c decays with N, which decreases with a characteristics time of 60 ps. As the pump power is raised, the maximum value of r_c attained in the process of the condensate formation first increases, has a maximum for $P = 2.3P_0$, and decreases at still higher powers. Note that the maximum value of r_c is almost equal to the size of the emitting spot. This means that the condensate occupies the entire excitation region. The decrease in r_c at high excitation powers can be related both to an increase in the energy of particle–particle interactions in the condensate [12] and to the stronger overheating of the exciton reservoir [14].

The expansion of coherence and the formation of a condensate are accompanied by narrowing of the polariton momentum distribution. This is illustrated by Fig. 3a, which shows the dynamics of the polariton momentum distribution for excitation densities of $1.3P_0$ and $3.4P_0$. The kinetics of the inverse width (FWHM) $1/\Delta k$ of the momentum distribution for three different excitation densities are shown in Fig. 3b by closed symbols. In an ideal Bose gas at equilibrium, the polariton momentum distribution function $f(k)$ and the spatial distribution of coherence $g^{(1)}(\Delta x)$ are related by the Fourier transform [13], whence a relation between r_c and Δk can be obtained. For a classical two-dimensional Bose gas below the BEC threshold, $f(k) \sim \exp(-k^2/2mT)$, $g^{(1)}(\Delta x) = \exp(-mT\Delta x^2/2)$, and, thus, $r_c\Delta k = 3.3$; above the BEC threshold, $f(k) \sim 1/(\exp(k^2/2mT - \mu/T) - 1) \approx 1/(k^2/2mT - \mu/T)$, $g^{(1)}(\Delta x) \sim \exp(-\Delta x\sqrt{2m|\mu|})$, and, thus, $r_c\Delta k \approx 2$. However, the product of r_c and Δk measured experimentally proves to be significantly larger than 3.3 at the time corresponding to the highest

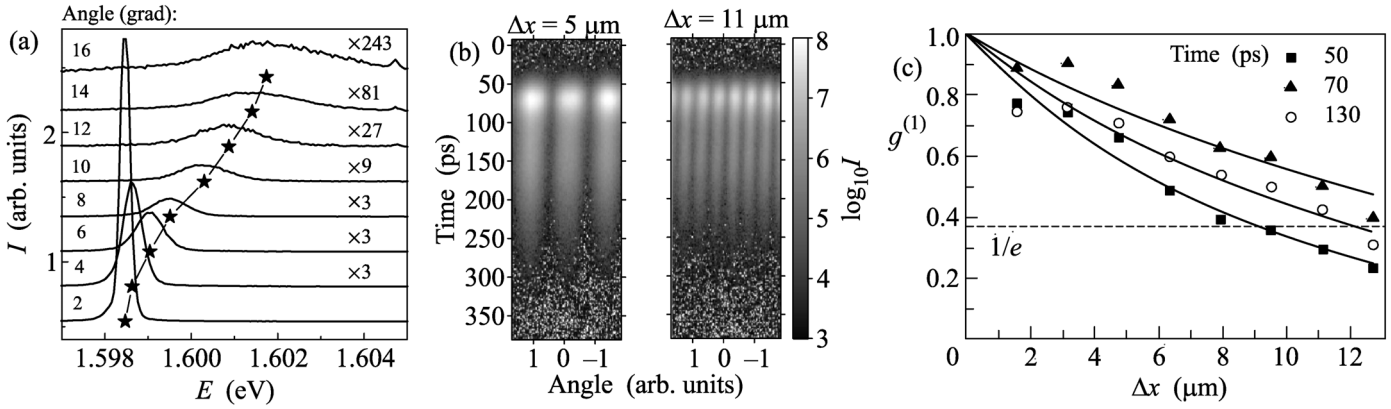

Fig. 1. (a) Time-integrated PL spectra of the sample recorded at different angles with respect to its normal. Asterisks show the positions of the spectral lines. The pump power is $P = 1.2P_0$. (b) The dynamics of the interference pattern for different distances Δx between the selected regions of the emitting spot. The pump power is $P = 3.4P_0$. (c) (Symbols) Coherence function versus the distance Δx at different times and (solid lines) the fits to these dependences by exponential functions. The pump power is $P = 3.4P_0$.

polariton density and decreases to 2 (for $P = 6.9P_0$) at the slow stage of the condensate kinetics. Apparently, this is caused by the strongly nonequilibrium character and the inhomogeneity of the system under consideration, as well as the nonideality of the polariton gas.

In the general case, the relation between the polariton momentum distribution and the spatial distribution of coherence depends on the size of the system and the spatial distribution of the phase $\varphi(x)$ of the condensate. The dependence of the far-field radiation intensity on the wave vector k, which (disregarding the weak variation of the photon Hopfield coefficient near the bottom of the LPB) represents the momentum distribution of polaritons, is determined by the interference of electric fields corresponding to different points of the condensate and is given by the formula

$$I(k) = \int_{-\infty}^{\infty}\int_{-\infty}^{\infty} E(x_1)E(x_2)g^{(1)}(|x_2 - x_1|) \times \exp[ik(x_2 - x_1) + i\varphi(x_2) - i\varphi(x_1)]dx_1dx_2. \quad (1)$$

This expression is obtained upon the summation of the electric-field amplitudes $E(x)$ along the PL spot and time averaging. Note that, in general, one needs to consider the integration with respect to two dimensions, x and y. However, it can be shown that, if the function $E(x, y)$ allows the separation of variables (e.g., when it is a Gaussian), this integral is reduced to Eq. (1), where $g^{(1)}$ is understood as the degree of coherence measured in a double-slit experiment. Equation (1) can also be used to calculate the intensity distribution in the experiment with two infinitely narrow slits spaced by Δx by substituting a field distribution of the form $E(x) = E(\Delta x/2)(\delta(x - \Delta x/2) + \delta(x + \Delta x/2))$.

We calculated the distribution $I(k)$ at different times under the following assumptions: the spatial coherence function can be written as $g^{(1)}(x) = \exp(-x/r_c)$, where r_c is determined from the experiment; the phase distribution is uniform, i.e., $\varphi(x) = \text{const}$; and the spatial distribution of the electric-field amplitude of the condensate is described by a Gaussian $\exp(-x^2/L^2)$. The size L of the sample area occupied by the condensate was determined by measuring the size of the magnified image of the condensate. For $P = 1.3P_0$, $3.4P_0$, and $6.9P_0$, this size was $L = 12$, 14, and 20 μm, respectively. The measured and calculated distributions $I(k)$ at time $t = 150$ ps for $P = 6.9P_0$ are plotted in the inset in Fig. 3b. The kinetic dependences of the inverse width $1/\Delta k$ characterizing the calculated distributions $I(k)$ are shown in Fig. 3b by open symbols. As one would expect, they reproduce to a large extent the kinetics of r_c (Fig. 2). At the same time, there are significant differences between the measured and calculated kinetic dependences of $1/\Delta k$ (Fig. 3b).

At a low excitation density of $1.3P_0$, the calculated and observed kinetics of $1/\Delta k$ are similar, but the calculated values exceed the measured ones by almost a factor of 2. At higher excitation densities, there are significant differences between the behaviors of the observed and calculated kinetics. For $P = 3.4P_0$, the measured dependence of $1/\Delta k$ exhibits at the first (fast) stage of the kinetics a short plateau followed by a rapid rise before entering a longer plateau at the second (slow) stage. Meanwhile, the calculated dependences of $1/\Delta k$ exhibit a sharp maximum at the fast stage of the kinetics and then, after an abrupt drop, enter a plateau at the slow stage (see Fig. 3b for $P = 3.4P_0$ and $6.9P_0$). The differences in the behaviors of the decay kinetics of $1/\Delta k$ for $t > 200$ ps are probably

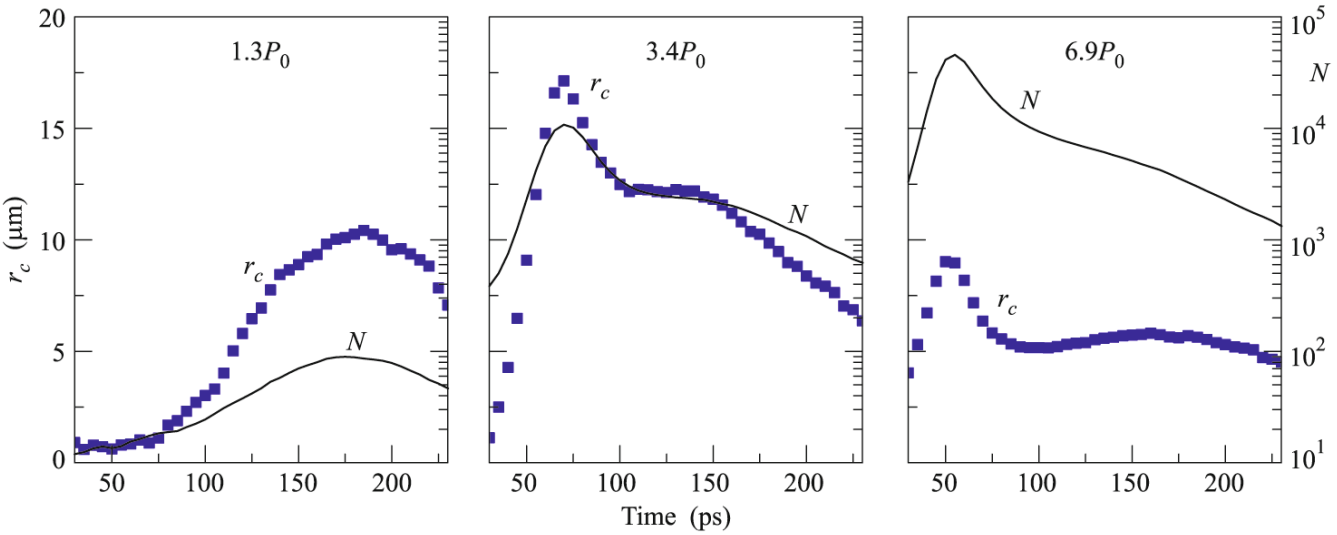

Fig. 2. (Color online) (Symbols, left scale) Kinetics of the coherence length and (lines, right scale) the total number of polaritons near the bottom of the LPB for different pump powers.

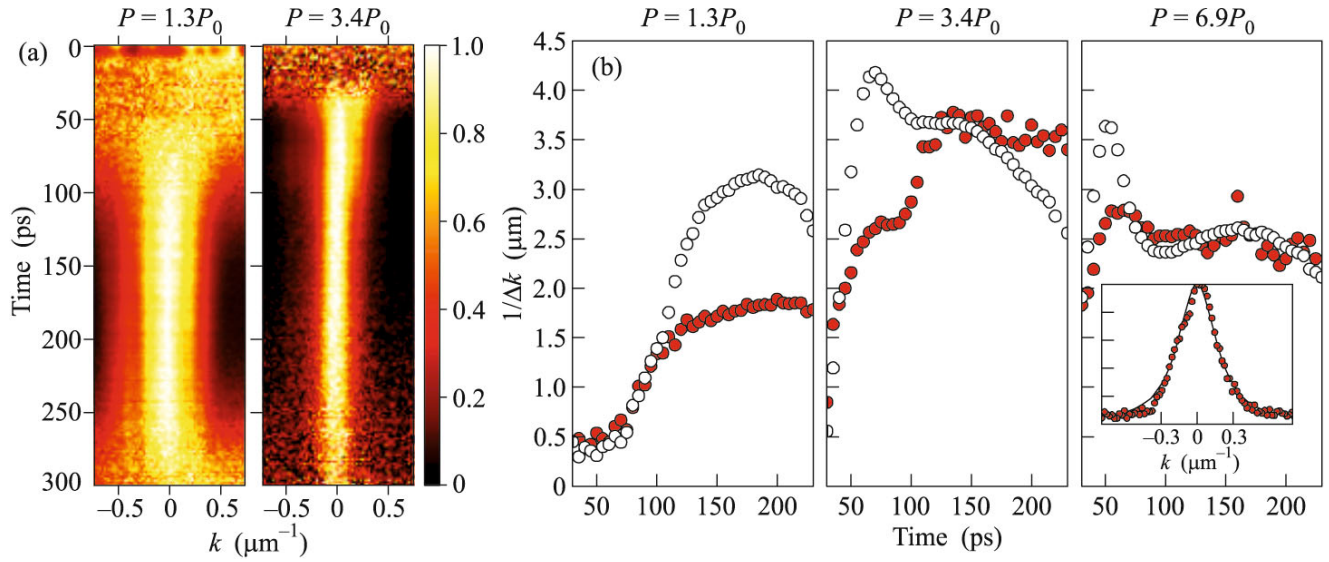

Fig. 3. (Color online) (a) Kinetics of the polariton distribution in k space for pump powers $P = 1.3P_0$ and $3.4P_0$. The distribution is normalized to the intensity maximum at each moment of time. (b) The kinetics of the inverse width of the polariton distribution in k space measured experimentally and calculated from the coherence function according to Eq. (1) (closed and open symbols, respectively). The inset shows the measured and calculated function $I(k)$ (symbols and solid line, respectively) for $P = 6.9P_0$ and $t = 150$ ps.

caused by the experimental uncertainty owing to the small PL intensity in this time range.

The discrepancies in the values of $1/\Delta k$ measured directly and calculated on the basis of the experimentally determined dependences $g^{(1)}(x)$ that occur at the fast stage of the kinetics are most probably related to the strong spatial nonuniformity of the phase of the condensate wavefunction in this time range, which was disregarded in the calculations. This nonuniformity causes a phase shift $\Delta\varphi$ between the areas of the condensate selected by the two slits, which, in the context of the measurements of $g^{(1)}(x)$, leads to a shift of the interference pattern without affecting its visibility. At the same time, phase nonuniformity causes significant broadening of the distribution $I(k)$. This can easily be seen upon substituting, e.g., a linearly varying phase $\varphi(x) \sim x$ in Eq. (1). This assumption is supported by the data in Fig. 4, which shows the kinetic dependences of the phase difference $\Delta\varphi$ between the regions of the condensate selected by the two slits. The values of $\Delta\varphi$ were determined from the shift of the interfer-

ence pattern. At the fast stage of the kinetics, $\Delta\varphi$ varies considerably, these variations being larger for larger distances Δx between the corresponding areas of the condensate. These results give evidence of the strong spatial nonuniformity of the phase. Upon the transition to the slow stage of the kinetics, the variation of $\Delta\varphi$ becomes much weaker, and a steady-state distribution of the phase sets in.

The spatial nonuniformity of the phase may originate from the inhomogeneity of the potential energy of polaritons in the microcavity plane, which may cause the formation of topological defects in the condensate, such as quantum vortices [3] and dark solitons [15]. Upon a round trip about the core of such a defect, the phase varies by 2π, and the defect size is determined by the healing length $\xi = \hbar/\sqrt{(2m\alpha N/S)}$ [15], where m is the polariton effective mass, α is the polariton–polariton interaction constant, and S is the area of the condensate. Thus, ξ determines the characteristic length scale upon which the phase varies by $\sim\pi$. Substituting numerical values of $m = 5 \times 10^{-32}$ g, $\alpha = 10^{-12}$ meV cm^2, and $S = 10^{-6}$ cm^2, we find that, for $P = 3.4P_0$, near the peak of the intensity, when $N \sim 10^4$, the healing length is $\xi = 8$ μm, which is noticeably smaller than the size of the area occupied by the condensate ($L = 14$ μm). Then, the phase nonuniformity resulting from the formation of topological defects may lead to the considerable broadening of the polariton momentum distribution. At the slow stage of the kinetics, $N \sim 2000$ and $\xi = 18$ μm. In this situation, the contribution of phase nonuniformity to the increase in Δk is much smaller.

Note that, at higher excitation densities, the formation of the condensate may originate in several areas of the microcavity simultaneously. This may also contribute to the nonuniformity of the phase: initially, phases in these areas are independent and equalize in the course of the condensate formation.

Thus, we have for the first time simultaneously measured the dynamic characteristics of the spatial coherence and the polariton momentum distribution under the conditions of polariton Bose condensation in a GaAs microcavity with embedded QWs. We have shown that, at sufficiently high densities of nonresonant excitation by picosecond light pulses, there are two stages in the dynamics of the total number of polaritons in the condensate. At the first, fast, stage, the coherence length increases abruptly and then decreases, following the corresponding changes in the number of polaritons occupying states near the LPB bottom. Meanwhile, the polariton momentum distribution exhibits steady narrowing that ceases only at the slow stage in the kinetics of the number of particles in the condensate. Apparently, the observed difference in the character of the dynamics of spatial coherence and polariton momentum distribution at the fast stage of the condensate kinetics is caused by spatial nonuniformity existing on this timescale in the distribution of the phase of the condensate wavefunction, which sets in (smoothens) much slower.

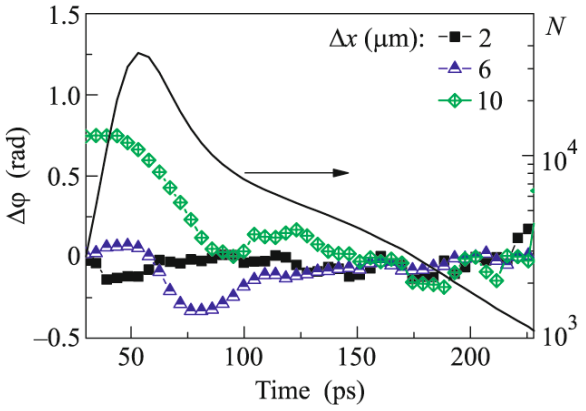

Fig. 4. (Color online) (Left scale, symbols) Kinetics of the phase difference $\Delta\varphi$ between the areas of the condensate selected by the two slits for different distances Δx and (right scale, solid line) the number of polaritons N near the bottom of the LPB. The phase difference is measured with respect to its value at time $t = 230$ ps. The excitation power is $P = 6.9P_0$.

We are deeply grateful to S.S. Gavrilov, N.A. Gippius, and S.I. Novikov for valuable advice and useful discussions. The study was supported by the Russian Foundation for Basic Research (project nos. 12-02-33091, 13-02-12197, and 14-02-01073) and the Presidium of the Russian Academy of Sciences. The work of V.V.B. was supported in part by a scholarship of the President of the Russian Federation.

REFERENCES

1. A. Imamoglu, R. J. Ram, S. Pau, and Y. Yamamoto, Phys. Rev. A **53**, 4250 (1996).
2. J. Kasprzak, M. Richard, S. Kundermann, A. Baas, P. Jeambrun, J. M. J. Keeling, F. M. Marchetti, M. H. Szymańska, R. André, J. L. Staehli, V. Savona, P. B. Littlewood, B. Deveaud, and Le Si Dang, Nature **443**, 409 (2006).
3. K. G. Lagoudakis, M. Wouters, M. Richard, A. Baas, I. Carusotto, R. André, Le Si Dang, and B. Deveaud-Plédran, Nature Phys. **4**, 706 (2008).
4. A. Amo, J. Lefrére, S. Pigeon, C. Adrados, C. Ciuti, I. Carusotto, R. Houdré, E. Giacobino, and A. Bramati, Nature Phys. **5**, 805 (2009).
5. K. G. Lagoudakis, B. Pietka, M. Wouters, R. André, and B. Deveaud-Plédran, Phys. Rev. Lett. **105**, 120403 (2010).
6. A. V. Larionov, V. D. Kulakovskii, S. Höfling, C. Schneider, L. Worschech, and A. Forchel, Phys. Rev. Lett. **105**, 256401 (2010).
7. M. Sich, D. N. Krizhanovskii, M. S. Skolnick, A. V. Gorbach, R. Hartley, D. V. Skryabin, E. A. Cerda-Méndez, K. Biermann, R. Hey, and P. V. Santos, Nature Photon. **6**, 50 (2012).
8. E. Kammann, T. C. H. Liew, H. Ohadi, P. Cilibrizzi, P. Tsotsis, Z. Hatzopoulos, P. G. Savvidis, A. V. Ka-

vokin, and P. G. Lagoudakis, Phys. Rev. Lett. **109**, 036404 (2012).

9. P. Bhattacharya, T. Frost, S. Deshpande, M. Z. Baten, A. Hazari, and A. Das, Phys. Rev. Lett. **112**, 236802 (2014).
10. G. Nardin, K. G. Lagoudakis, M. Wouters, M. Richard, A. Baas, R. André, Le Si Dang, B. Pietka, and B. Deveaud-Plédran, Phys. Rev. Lett. **103**, 256402 (2009).
11. H. Ohadi, E. Kammann, T. C. H. Liew, K. G. Lagoudakis, A. V. Kavokin, and P. G. Lagoudakis, Phys. Rev. Lett. **109**, 016404 (2012).
12. V. V. Belykh, N. N. Sibeldin, V. D. Kulakovskii, M. M. Glazov, M. A. Semina, C. Schneider, S. Höfling, M. Kamp, and A. Forchel, Phys. Rev. Lett. **110**, 137402 (2013).
13. H. Deng, G. S. Solomon, R. Hey, K. H. Ploog, and Y. Yamamoto, Phys. Rev. Lett. **99**, 126403 (2007).
14. V. V. Belykh and D. N. Sob'yanin, Phys. Rev. B **89**, 245312 (2014).
15. A. A. Demenev, S. S. Gavrilov, A. S. Brichkin, A. V. Larionov, and V. D. Kulakovskii, JETP Lett. **100**, 523 (2014).

Translated by M. Skorikov